A Hierarchical Bayesian Model Accounting for Endmember Variability and Abrupt Spectral Changes to Unmix Multitemporal Hyperspectral Images – Supplementary materials

Pierre-Antoine Thouvenin, *Member, IEEE*, Nicolas Dobigeon, *Senior Member, IEEE* and Jean-Yves Tourneret, *Senior Member, IEEE*

This document contains supplementary material associated with the paper "A Hierarchical Bayesian Model Accounting for Endmember Variability and Abrupt Spectral Changes to Unmix Multitemporal Hyperspectral Images". Section I gives further details on the choice of the hyperparameters reported in the paper in Table I, whereas Section II provides a complementary illustration to substantiate the interest of the proposed abundance prior. Section III finally reports the abundance maps and endmembers extracted at each time instant by the different methods for the synthetic dataset composed of 3 endmembers.

I. Details on the values chosen for the hyperparameters

The initial values chosen for the parameters given in the paper in Table I are based on the following considerations.

(a) The initial noise variance σ_t^2 reflects a typical order of magnitude of the SNR (HS images are typically known to have an SNR around $30\,\mathrm{dB}$).
(b) The initial outlier variance s_t^2 has been taken an order of magnitude greater than σ_t^2 to ensure outlier contributions that can be captured by the algorithm.
(c) The initial variability variance $\psi_{\ell,r}^2$, which controls the temporal smoothness of the variability term, can be *a priori* chosen of the same order of magnitude as s_t^2.
(d) The granularity parameters β_t were initially selected to reflect the practitioner's prior knowledge on the smoothness of the outlier spatial support. A value between 1 and 2 (i.e., above the phase-transition temperature of the Ising MRF [1]) is particularly appropriate for natural scenes, in which the observed materials exhibit a relatively smooth spatial distribution.

Similarly, the values of the fixed parameters given in the paper in Table I have been selected as follows.

(a) ε_n^2, which controls the confidence given to the abundance smoothness prior, has been fixed by cross-validation (i.e., based on the estimation results obtained by multiple runs for different values);
(b) Since no specific prior knowledge is available on the endmembers, the endmember variance ξ is chosen sufficiently large (typically equal to 1) to ensure the endmember prior is weakly informative;
(c) ν, which controls the energy of the variability captured by the algorithm, has been set by cross validation;
(d) Given the absence of specific prior knowledge on the outlier variances s_t^2, the variability variances $\psi_{\ell,r}^2$ and the noise variances σ_t^2, the hyperparameters $a_{\mathbf{s}}, a_\Psi, a_\sigma, b_{\mathbf{s}}, b_\Psi, b_\sigma$ are set to a small value (typically 10^{-3}) to ensure the chosen conjugate inverse-gamma priors are uninformative [2];
(e) The number of Monte-Carlo and burn-in iterations, respectively denoted by N_{MC} and N_{bi}, are set according to a classical convergence diagnosis, namely the potential scale reduction factor (PSRF) [3].

II. Complementary illustration for the proposed abundance prior

In this section, a complementary figure (Fig. 1) illustrates the interest of considering the proposed abundance prior whenever outliers are observed in the MTHS image for synthetic dataset composed of $R = 3$ endmembers. This illustration is further substantiated by the estimation metrics detailed for each time instant in Table I.

III. Complementary figures for the results obtained on synthetic data ($R = 3$)

The endmembers and the abundance maps extracted by the different unmixing methods at the each time instants are reported in Figs. 2 to 5.

This work was supported in part by the Hypanema ANR Project no. ANR-12-BS03-003, by the MapInvPlnt ERA-NET MED Project no. ANR-15-NMED-0002-02, by the Thematic Trimester on Image Processing of the CIMI Labex under Grant ANR-11-LABX-0040-CIMI within the Program ANR-11-IDEX-0002-02 and by the Direction Générale de l'Armement, French Ministry of Defence.

The authors are with the University of Toulouse, IRIT/INP-ENSEEIHT, 31071 Toulouse, France. (e-mail: {pierreantoine.thouvenin, Nicolas.Dobigeon, Jean-Yves.Tourneret}@enseeiht.fr

References

[1] M. Pereyra, N. Dobigeon, H. Batatia, and J.-Y. Tourneret, "Computing the Cramer-Rao bound of Markov random field parameters: Application to the Ising and the Potts models," *IEEE Signal Process. Lett.*, vol. 21, no. 1, pp. 47–50, Jan. 2014.
[2] Y. Altmann, S. McLaughlin, and A. O. Hero, "Robust linear spectral unmixing using anomaly detection," *IEEE Trans. Comput. Imag.*, vol. 1, no. 2, pp. 74–85, Jun. 2015.
[3] A. Gelman and D. B. Rubin, "Inference from iterative simulation using multiple sequences," *Statistical Science*, vol. 7, no. 4, pp. 457–511, 1992.

Fig. 1. Evolution of the abundance corresponding to a pixel in which outliers are observed at several time instants (indicated by vertical dotted lines). The abundance coefficient estimated at each time instant by the different unmixing strategies are reported in different colors. The proposed method proves to be particularly appropriate to mitigate the errors induced by the presence of outliers.

Fig. 2. Endmembers ($\mathbf{m}_r$, red lines) and their variants affected by variability ($\mathbf{m}_r + \mathbf{dm}_{r,t}$, blue dotted lines) recovered by the different methods from the synthetic mixtures with $R = 3$. Each row of the figure corresponds to the endmembers extracted for the 3 materials by each algorithm. Signatures corresponding to different time instants are represented on a single figure to better appreciate the variability recovered from the data. The spectra represented in black in Figs. 2a, 2b, 2d, 2e and 2h correspond to signatures corrupted by outliers.

TABLE I

DETAILED TABLE OF RESULTS OBTAINED ON THE SYNTHETIC DATA COMPOSED OF $R = 3$ ENDMEMBERS. THE CRITERION $\mathrm{aSAM}(\mathbf{M}_t)$ DENOTES THE AVERAGE SPECTRAL ANGLE MAPPER BETWEEN THE GROUND TRUTH PERTURBED ENDMEMBERS $\mathbf{M}_t = \mathbf{M} + \mathbf{dM}_t$ AND THE ESTIMATED PERTURBED ENDMEMBERS AT TIME INSTANT t. THE TIME INSTANTS REPRESENTED WITH $*$ DENOTE IMAGES CONTAINING OUTLIERS.

	t	1	2*	3	4	5*	6*	7	8	9	10*
GMSE($\mathbf{A}_t$)	VCA	1.835e-03	3.764e-02	2.379e-03	1.644e-03	5.942e-02	6.598e-02	1.823e-03	1.963e-03	1.228e-03	5.849e-02
	SISAL	1.088e-04	3.631e-02	4.532e-05	3.667e-04	3.973e-02	4.002e-02	1.304e-04	1.136e-04	1.708e-04	4.242e-02
	RLMM	1.689e-03	3.788e-02	2.092e-03	1.526e-03	4.924e-02	5.442e-02	1.716e-03	1.859e-03	1.188e-03	5.242e-02
	OU	9.990e-04	1.438e-02	9.873e-04	9.541e-04	9.571e-03	8.797e-03	8.247e-04	8.437e-04	9.699e-04	3.633e-03
	MCMC	4.826e-04	2.715e-03	4.899e-04	5.583e-04	1.880e-03	1.780e-03	9.692e-04	1.201e-03	1.716e-03	3.104e-03
aSAM($\mathbf{M}_t$)	VCA	2.095e+00	1.840e+01	3.085e+00	2.560e+00	1.055e+01	1.100e+01	2.622e+00	2.706e+00	2.252e+00	1.035e+01
	SISAL	4.842e-01	2.672e+01	2.669e-01	7.102e-01	1.055e+01	1.004e+01	5.483e-01	5.191e-01	5.956e-01	9.231e+00
	RLMM	1.502e+00	2.134e+01	1.647e+00	1.401e+00	8.894e+00	9.427e+00	1.782e+00	1.665e+00	1.520e+00	8.874e+00
	OU	1.231e+00	4.402e+00	1.317e+00	1.346e+00	3.197e+00	2.984e+00	1.312e+00	1.292e+00	1.353e+00	1.785e+00
	MCMC	1.522e+00	1.461e+00	8.965e-01	6.649e-01	7.913e-01	8.633e-01	1.055e+00	1.226e+00	1.679e+00	2.797e+00
RE	VCA	1.308e-04	5.450e-04	2.119e-04	1.942e-04	6.402e-04	5.543e-04	3.400e-04	2.817e-04	3.416e-04	6.675e-04
	SISAL	1.252e-04	2.438e-04	1.621e-04	1.635e-04	2.714e-04	1.824e-04	3.323e-04	2.110e-04	3.343e-04	2.500e-04
	RLMM	1.844e-04	7.596e-04	2.593e-04	2.608e-04	6.193e-04	4.322e-04	6.139e-04	3.579e-04	6.193e-04	4.894e-04
	OU	1.254e-04	4.108e-04	1.624e-04	1.637e-04	3.367e-04	2.458e-04	3.325e-04	2.113e-04	3.346e-04	2.843e-04
	MCMC	1.252e-04	1.238e-04	1.621e-04	1.635e-04	2.060e-04	1.307e-04	3.314e-04	2.109e-04	3.319e-04	2.102e-04
aSAM($\mathbf{Y}_t$)	VCA	1.904e+00	3.025e+00	2.387e+00	2.284e+00	3.844e+00	3.480e+00	2.954e+00	2.605e+00	2.930e+00	3.523e+00
	SISAL	1.872e+00	2.351e+00	2.099e+00	2.093e+00	2.557e+00	2.059e+00	2.929e+00	2.321e+00	2.904e+00	2.392e+00
	RLMM	1.964e+00	3.422e+00	2.231e+00	2.220e+00	3.040e+00	2.469e+00	3.170e+00	2.480e+00	3.150e+00	2.650e+00
	OU	1.873e+00	2.527e+00	2.100e+00	2.095e+00	2.603e+00	2.084e+00	2.930e+00	2.322e+00	2.905e+00	2.414e+00
	MCMC	1.872e+00	1.785e+00	2.099e+00	2.093e+00	2.303e+00	1.828e+00	2.925e+00	2.320e+00	2.892e+00	2.282e+00

Fig. 3. Abundance map of the endmember 1 recovered by the different methods (in each row) at each time instant (given in column) for the experiment with $R = 3$ [the different rows correspond to the true abundances, VCA/FCLS, SISAL/FCLS, RLMM, OU and the proposed method]. The images delineated in red show that several methods are highly sensitive to the presence of outliers, and the time instants represented with $*$ denote images containing outliers.

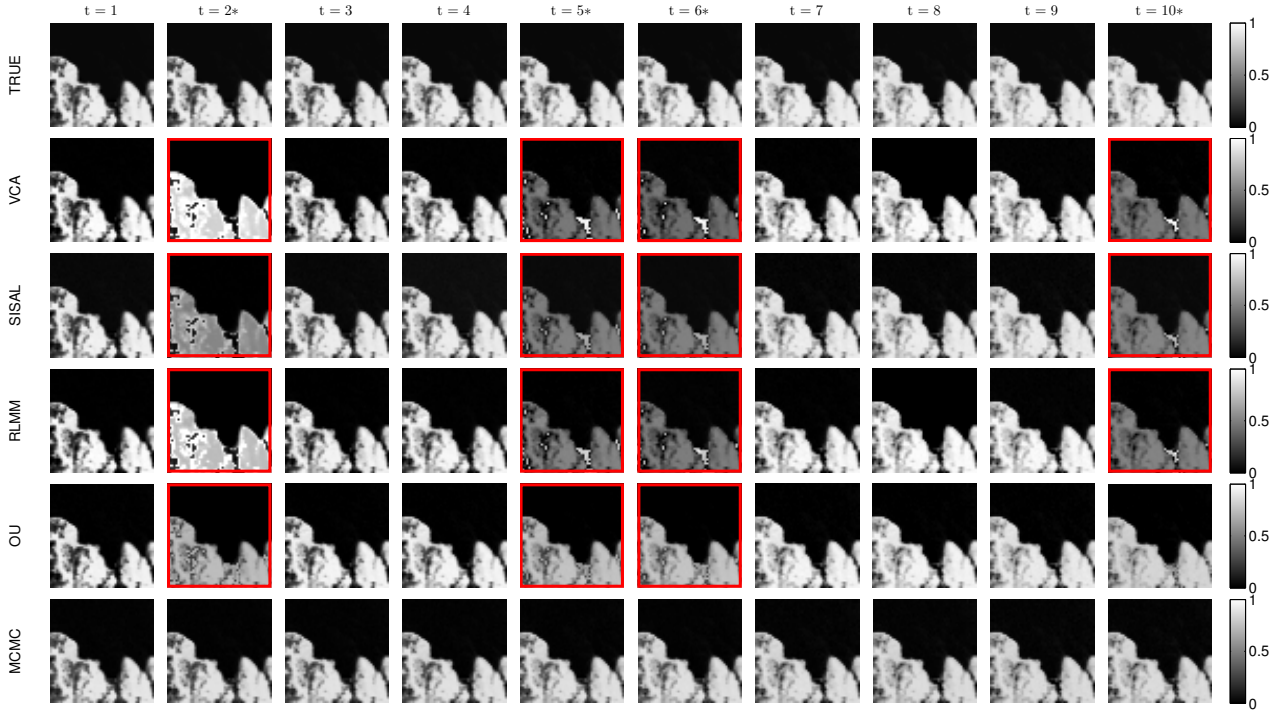

Fig. 4. Abundance map of the endmember 2 recovered by the different methods (in each row) at each time instant (given in column) for the experiment with $R = 3$ [the different rows correspond to the true abundances, VCA/FCLS, SISAL/FCLS, RLMM, OU and the proposed method]. The images delineated in red show that several methods are highly sensitive to the presence of outliers, and the time instants represented with $*$ denote images containing outliers.

Fig. 5. Abundance map of the endmember 3 recovered by the different methods (in each row) at each time instant (given in column) for the experiment with $R = 3$ [the different rows correspond to the true abundances, VCA/FCLS, SISAL/FCLS, RLMM, OU and the proposed method]. The images delineated in red show that several methods are highly sensitive to the presence of outliers, and the time instants represented with $*$ denote images containing outliers.